PNAS RESEARCH ARTICLE | MEDICAL SCIENCES

The dichotomous roles of microbial-modified bile acids 7-oxo-DCA and isoDCA in intestinal tumorigenesis

Xingchen Dong[a], Fei Sun[a], Henry Secaira-Morocho[b], Alisa Hui[c], Ke Wang[a], Chunmiao Cai[a], Shirsa Udgata[d], Brian Low[c], Songlin Wei[a], Xinyi Chen[a], Ming Qi[a], Cheri A. Pasch[d], Wei Xu[e,f], Jiaoyang Jiang[a], Qiyun Zhu[b], Tao Huan[c], Dustin A. Deming[d,e,f], and Ting Fu[a,f,1]

Affiliations are included on p. 12.

Edited by Antonio Moschetta, University of Bari, Bari, Italy; received October 10, 2023; accepted September 16, 2024 by Editorial Board Member David J. Mangelsdorf

The gut microbiota has a significant impact on the development and function of intestinal epithelial cells (IECs) by modifying bile acid (BA) metabolites. Recently, specific gut microbiome-derived BAs, such as 7-oxo-deoxycholic acid (7-oxo-DCA) and isodeoxycholic acid (isoDCA), have been identified to be shifted inversely in colitis and hepatic liver diseases. Although the responsible gut microbes have been identified, metabolites' effects on IECs remain largely unclear. We found that although high-fat diet treatment in mice elevated both 7-oxo-DCA and isoDCA levels, during intestinal tumorigenesis, 7-oxo-DCA levels rise while isoDCA levels decrease. Interestingly, 7-oxo-DCA promotes cancer cell growth, while isoDCA suppresses it. Moreover, 7-oxo-DCA promotes whereas isoDCA inhibits the proliferation of intestinal stem cells in organoids derived from WT and *APC*$^{Min/+}$ mice, as well as in patient-derived colon cancer organoids. The *APC*$^{Min/+}$ mice administered with 7-oxo-DCA heightened gut permeability and increased tumor burden, whereas isoDCA protected gut barrier and reduced tumor loads. Both BAs reshape the BA pool and shifted gut microbiome. Mechanistically, we identified 7-oxo-DCA as a natural antagonist of Farnesoid X Receptor (FXR) to downregulate FXR signaling, as opposed to isoDCA, which is a potent FXR agonist to upregulate FXR signaling. In conclusion, we unveiled the opposing roles of 7-oxo-DCA and isoDCA to promote or inhibit intestinal tumorigenesis, respectively. Manipulating the BA–FXR axis during tumor initiation and progression holds great promise for developing innovative diagnostic and therapeutic approaches for the treatment of colorectal cancer.

bile acids | nuclear receptor FXR | colorectal cancer

Significance

Colorectal cancer (CRC) stands as the third leading cause of cancer-linked mortality and second-most prevalent in the United States. Bile acids (BAs) could serve as either CRC promoters or inhibitors, depending on their differential interaction with the nuclear receptor Farnesoid X Receptor (FXR). Genetic factors, diet, and the gut microbiota are presumed to synchronize the BA-mediated tumorigenic effect. Our study reveals differential roles of two microbiome-derived, structurally related BAs, 7-oxo-deoxycholic or isodeoxycholic acid, in promoting or inhibiting tumorigenesis by differentially modulating FXR pathway.

Colorectal cancer (CRC) affects over 100,000 patients annually and stands as the third leading contributor to cancer-related fatalities in the United States (1). As an interface between the host and the environment, the gut undertakes vital physiological functions like absorbing nutrients and water (1, 2). Furthermore, the gut must maintain homeostasis by accommodating diverse diets and commensal microbes while adeptly safeguarding against injury and pathogens (1, 3). Bile acids (BAs), derived from cholesterol, play a pivotal role by emulsifying dietary lipids for efficient absorption (4). Within the liver–gut axis, these BAs actively circulate, orchestrating postprandial responses (2, 5–7). Serving as early dietary sensors, BAs transmit alterations in nutrition and the microbiome to intestinal epithelial cells (IECs) while also coordinating shifts in immune cells, partly via modulating the activities of Farnesoid X Receptor (FXR), the natural nuclear receptor of BAs (1, 8–11).

BAs dysregulation is a convergent point of genetic and dietary risk factors of CRC (8, 12–15). Previously, we identified abnormally high levels of host BAs like tauro-beta-muricholic acid (T-β-MCA), which caused DNA damage, stimulated the proliferation of Lgr5-expressing intestinal stem cells (ISCs), and propelled malignant transformation during CRC progression (8, 16). Further investigations revealed T-β-MCA as an antagonist of FXR. Its oncogenic effects were mediated through the inhibition of FXR signaling and the activation of Wnt signaling pathways (17). This finding underscored the potential utility of distinct BAs in diagnosis and therapeutic implication of the BAs–FXR axis in CRC (2, 10).

Recently, a couple of studies have unveiled novel roles of various microbial BAs in influencing intestinal immune cells (18–22). For instance, one investigation disclosed elevated levels of iso-, 3-oxo-, allo-, 3-oxoallo-, and isoallolithocholic acid (LCA) in centenarians, potentially mitigating the risk of pathobiont infections (23). In a different study, it was demonstrated that 3-oxoLCA and isoalloLCA hinder Th17 cell differentiation, while isoalloLCA enhances Treg differentiation (19). Another study revealed that

Author contributions: X.D. and T.F. designed research; X.D., F.S., A.H., S.W., X.C., M.Q., and T.F. performed research; H.S.-M., K.W., C.C., S.U., C.A.P., J.J., Q.Z., T.H., and D.A.D. contributed new reagents/analytic tools; X.D., H.S.-M., A.H., K.W., B.L., W.X., Q.Z., T.H., and T.F. analyzed data; D.A.D. provide valuable scientific insight; and X.D. and T.F. wrote the paper.

The authors declare no competing interest.

This article is a PNAS Direct Submission A.M. is a guest editor invited by the Editorial Board.

[1]To whom correspondence may be addressed. Email: ting.fu@wisc.edu.

This article contains supporting information online at https://www.pnas.org/lookup/suppl/doi:10.1073/pnas.2317596121/-/DCSupplemental.

Published November 12, 2024.

3β-hydroxydeoxycholic acid (3-epi-DCA) boosts Foxp3 induction through its interaction with dendritic cells (DCs) (20). Furthermore, a recent research endeavor reported that an inulin fiber diet reshapes the mouse microbiota composition, triggering intestinal type 2 inflammation, and surged levels of microbiota-derived BAs, notably including 7-oxo-deoxycholic acid (7-oxo-DCA) (24). Interestingly, 7-oxo-DCA exhibited significant positive correlations with diseases linked to BAs disorders, including nonalcoholic fatty liver disease (NAFLD), hepatic fibrosis, nonalcoholic steatohepatitis (NASH), ballooning, and hepatocellular carcinoma (HCC) (25, 26). In the context of metabolite profiling within the Integrative Human Microbiome Project (HMP2) cohort, it was observed that oxo-DCA levels rise in patients with Crohn's disease (CD), while isodeoxycholic acid (isoDCA) levels decline (18). Although the gut microbes responsible for interconverting 3-oxo-DCA, 7-oxo-DCA, and isoDCA have been identified (27–31), the precise impacts of these microbial BAs on IECs, and the underlying mechanisms influencing CRC progression remain largely elusive.

Disrupted BAs homeostasis could cause the imbalances in the gut microbiome and affect the activation of FXR within the gut. Therefore, the present study was performed to delineate the role of these BAs in IECs and the associated molecular mechanisms in the tumorigenesis of CRC.

Results

7-oxo-DCA Acts as a Neutral Antagonist and isoDCA Acts as Potent Agonist of FXR. Our previous research delved into the influence of genetic and dietary changes on CRC progression, examining the metabolite perspective (8). Employing untargeted metabolomic profiling on serum and cecum samples from four distinct mouse groups—Wild-type (WT) on Normal Diet (ND, as a control), WT on High-Fat Diet (HFD, as an obesity model), and a genetic mutated $APC^{Min/+}$ (a truncating mutation in the Apc gene) mice on ND (representing an adenoma model), and $APC^{Min/+}$ mice on HFD (indicating an adenocarcinoma model)—we pinpointed specific metabolic shifts linked to CRC development and unearthed potential biomarkers relevant to CRC progression (8, 32). Among the altered metabolites, we made an interesting finding regarding certain microbial BAs, particularly 7-oxo-DCA and isoDCA (Fig. 1*A* and *SI Appendix*, Fig. S1*A*). Specifically, 7-oxo-DCA showed increased levels in the cecum samples of $APC^{Min/+}$ mice on a ND compared to WT mice (Fig. 1*B*), while isoDCA decreased (Fig. 1*C*). Furthermore, a HFD elevated 7-oxo-DCA concentration in both WT and $APC^{Min/+}$ mice (Fig. 1*B*). Interestingly, previous research has consistently reported abnormally elevated 7-oxo-DCA levels among patients with conditions like NAFLD, NASH, liver cancer (25, 26). Exploring metabolomics data of cecum samples from different stages of UC patients also unveiled a progressive rise of 7-oxo-DCA levels across inactive, mild, and moderate/severe states, along with a progressive decline of isoDCA (Fig. 1 *D* and *E*). Additional exploring the HMP2 IBD cohort also unveiled a progressive rise oxo-DCA levels across healthy individuals, as well as among those with nondysbiotic and dysbiotic CD, along with a progressive decline of isoDCA (*SI Appendix*, Fig. S1*B*) (18). Notably, these disorders share a common characteristic of BAs dysregulation. This compelling connection underscores the potential significance of 7-oxo-DCA in driving the progression of CRC, a condition also marked by BAs dysregulation.

Subsequently, we aimed to assess the biological activity of the identified microbial BAs, 7-oxo-DCA and isoDCA. To accomplish this, we employed a luciferase reporter plasmid (FXRE-Luc) containing a FXR-response element (FXRE). HEK293 cells were cotransfected with human or mouse FXR: RXR in a 1:1 ratio alongside FXRE-Luc plasmids. Cells were then exposed to increasing concentrations of 7-oxo-DCA or isoDCA, cotreated with the FXR synthetic agonist, GW4064 (Fig. 1*F* and *SI Appendix*, Fig. S1*C*), or the FXR antagonist, Dy268 (Fig. 1*G* and *SI Appendix*, Fig. S1*D*). Our findings revealed that 7-oxo-DCA acted as a neutral antagonist of FXR, failing to activate FXR and even reducing GW4064-induced activation (Fig. 1*F*). In contrast, isoDCA exhibited robust FXR agonistic activity, effectively activating FXR and counteracting Dy268's inhibitory effect on FXR (Fig. 1*G*). Notably, isoDCA reversed the inhibitory impact of 7-oxo-DCA on FXR (Fig. 1*H*) and demonstrated greater FXR activation potency compared to CDCA, a recognized potent natural BA FXR agonist (*SI Appendix*, Fig. S1*E*). In addition, we performed similar activation and competition assays on 3-oxo-DCA and DCA, indicating that DCA functions as a mild FXR antagonist, while 3-oxo-DCA acts as a mild FXR agonist (*SI Appendix*, Fig. S1 *F–H*). We further assessed the dose-dependent inhibitory effects of 7-oxo-DCA and activated effects of isoDCA on FXRE-Luc activation, determining a half-maximal inhibitory concentration (IC50) of 13.795 μM for 7-oxo-DCA and a half-maximal effective concentration (EC50) of 4.384 μM for isoDCA (Fig. 1 *I* and *J*). Notably, both 7-oxo-DCA and isoDCA did not change TGR5 activities, suggesting a preference for FXR over TGR5 in IECs (*SI Appendix*, Fig. S1*I*) (15).

Furthermore, ligand docking assays explored these BAs' binding interactions with human and mouse FXR. The results demonstrated that isoDCA exhibited a notably higher binding affinity for human FXR in comparison to 7-oxo-DCA (Fig. 1*K*), a pattern closely resembling that of CDCA (Fig. 1*L*), which stands as the most potent endogenous BA in hostto activate FXR. A similar trend was discerned when assessing 7-oxo-DCA and isoDCA, in contrast to CDCA in rat FXR binding (*SI Appendix*, Fig. S1*J*). Of note, isoDCA is a more potent human FXR agonist, compared to another microbial BA, 3-epi-DCA (*SI Appendix*, Fig. S1*K*). In addition, 3-oxo-DCA has stronger binding affinity to human FXR, than 3-epi-DCA (*SI Appendix*, Fig. S1*L*). Collectively, these findings suggest that 7-oxo-DCA functions as a neutral FXR antagonist, while isoDCA acts as a potent FXR agonist.

7-oxo-DCA Promotes Cancer Cell Growth while isoDCA Suppresses It. In our previous study (8), we found that FXR modulation influenced cancer cell growth, with FXR antagonists promoting growth and FXR agonists inhibiting it. This led us to investigate how 7-oxo-DCA, an FXR antagonist, and isoDCA, an FXR agonist, might impact cancer cell growth. To delve into this, we performed cell viability assays on human CRC cell lines, HCT116, and HT29. These cells were exposed to increasing doses of DCA, 3-oxo-DCA, 7-oxo-DCA, and isoDCA for 24 h, and cell growth was quantified through ATP production. Our findings revealed that 7-oxo-DCA dose-dependently promoted cancer cell growth, while isoDCA dose-dependently suppressed it (Fig. 2*A* and *SI Appendix*, Fig. S3*A*). In crystal violet assays, 7-oxo-DCA consistently induced significant cell growth, whereas isoDCA notably inhibited growth in both HCT116 and HT29 cells (Fig. 2*B* and *SI Appendix*, Fig. S3*B*). The results were quantified based on OD570nm readings. Through the wound healing assay, we observed that 3-oxo-DCA increased migratory and invasive potential in HCT116 and HT29 cells, whereas DCA and isoDCA decreased it (Fig. 2*C* and *SI Appendix*, Fig. S3*C*). Intriguingly, the effects of 7-oxo-DCA on both cell lines were limited, suggesting its potential role in promoting tumorigenesis during the initiation phase. To investigate the effects of 7-oxo-DCA and isoDCA on CRC cell growth through FXR modulation, we analyzed gene expression in HCT116 and HT29 cells, both with their endogenous FXR levels and with lentivirus-mediated overexpression of FXR (*SI Appendix*,

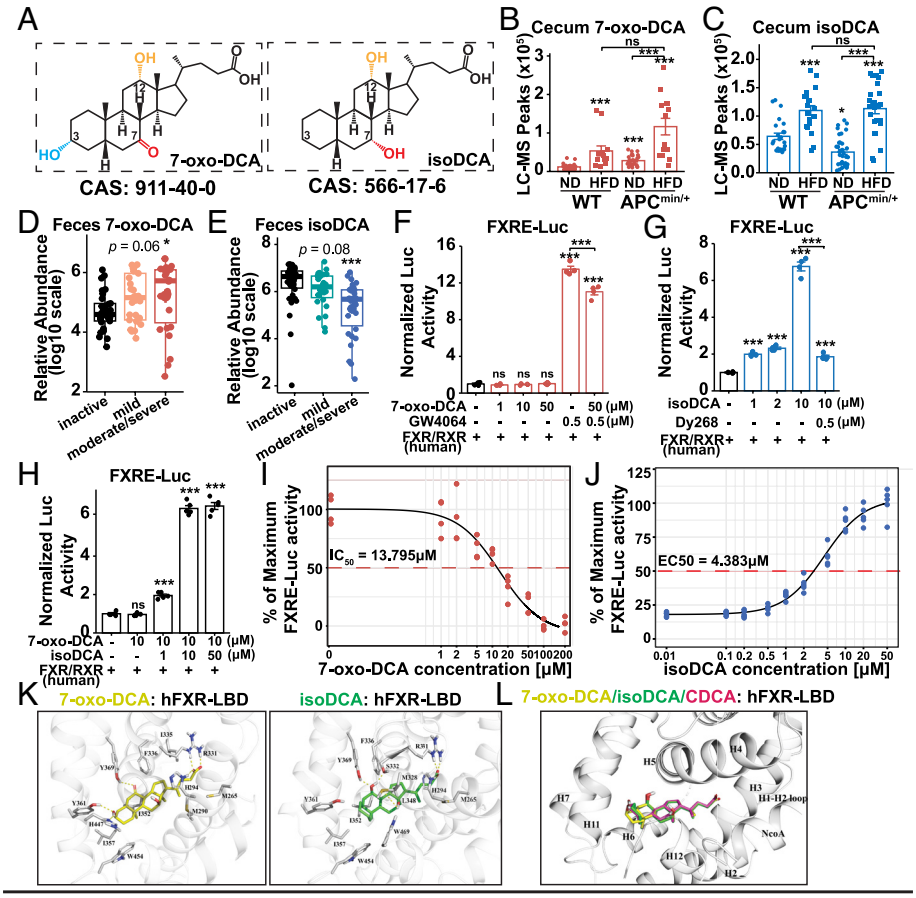

Fig. 1. 7-oxo-DCA aberrantly elevated in obese and CRC mouse models and patients. (*A*) The chemical structure of 7-oxo-DCA and isoDCA. (*B* and *C*) The levels of 7-oxo-DCA and isoDCA in the cecum samples of WT and *APC*$^{Min/+}$ mice maintained on a ND and a HFD, measured by LC-MS. (*D* and *E*) Metabolomics data from UC patients. Data were downloaded from the Metabolomics Workbench (https://www.metabolomicsworkbench.org/, Study ID: ST002470 for Blood; ST002471 for Feces). Relative abundances of 7-oxo-DCA (*D*) and isoDCA (*E*) from the feces are presented. (*F–H*) FXRE-Luc, a luciferase reporter gene functionally linked to an FXR-responsive element; plasmids expressing exogenous human FXR and RXR were cotransfected into HEK293 cells. After 24 h, cells were treated with the indicated concentration of 7-oxo-DCA and FXR agonist GW4064 (*F*), isoDCA and FXR antagonist Dy268 (*G*), and 7-oxo-DCA and isoDCA (*H*). Luciferase activities were measured 24 h later after treatment. (*I* and *J*) HEK293 cells were cotransfected with FXRE-Luc and human FXR/RXR-expressing plasmids. After 24 h, cells were treated with 0.1 μM GW4064 with indicated 7-oxo-DCA concentration, and luciferase activities were measured 24 h posttreatment. The luciferase activity in the GW4064 treatment group is denoted as the maximum activity (*I*), determining a half-maximal inhibitory concentration (IC50) of 13.795 μM for 7-oxo-DCA. Cells, after 24 h transfection, were treated with indicated concentrations of isoDCA without GW4064, and FXRE luciferase activities were measured 24 h later (*J*), determining a half-maximal effective concentration (EC50) of 4.384 μM for isoDCA. Independent biological replicates (n = 4) were analyzed, and half-maximum activities were determined using curve fitting by R 4.1.2. (*K* and *L*) Binding modes of human FXR-LBD (PDB 6HL1) agonist 7-oxo-DCA (yellow, −10.1 kcal/mol) (*I*), isoDCA (green, −11.3 kcal/mol) (*K*), and CDCA (magenta, −11.9 kcal/mol) (*L*). Key protein regions affected by ligand binding are highlighted. The critical polar residues and main hydrophobic residues in the pocket are labeled. The hydrogen bonds are shown in the yellow dash line. Three BAs bind at same pocket surrounded by the helix 2, 3, 5, 6, 11 and the loop connecting helix 1 and 2. The carboxyl group in three structures point to the same orientation and participate in hydrogen bonding with H294 and R331 as well as salt bridges. The 7-hydroxyl group of isoDCA participates in two hydrogen bonding interactions (S332 and Y369) as hydrogen donor and acceptor, respectively. The 7-carbonyl group of 7-oxo-DCA forms one hydrogen bond with Y369, making it a weaker binder compared with isoDCA. The hydrogen bonding interaction between 12-hydroxyl group of isoDCA and M328 contributes to its binding with FXR-LBD. All experiments were repeated three times independently, and representative data are shown as the mean ± SEM. For two-group comparison, Student's unpaired *t* tests were applied. For more than two group comparisons, the one-way ANOVA test followed by multiple comparisons was applied. *$P < 0.05$; **$P < 0.01$; ***$P < 0.005$; ns: not significant.

Fig. S2 *C–E*), after treating them with increasing doses of these BAs. As expected, 7-oxo-DCA significantly dampened FXR expression and its target genes (Fig. 2*D* and *SI Appendix*, Figs. S2*A* and S3 *D* and *E*), while isoDCA notably activated them (Fig. 2*D* and *SI Appendix*, Figs. S2*B* and S3 *D* and *E*) in both HCT116 and HT29 cells. Aligning with the aforementioned cell growth data, genes associated with cell cycling and the Wnt signaling pathway were upregulated by 7-oxo-DCA but downregulated by isoDCA (Fig. 2*D* and *SI Appendix*, Figs. S2 *A* and *B* and S3 *D* and *E*). Overall, these findings highlight that 7-oxo-DCA, functioning as an FXR antagonist, propels cancer cell growth, whereas isoDCA, a potent FXR agonist, suppresses growth.

7-oxo-DCA Stimulates ISCs' Proliferation while isoDCA Inhibits It. To comprehensively assess the influence of microbial BAs on intestinal cell growth, we employed primary intestinal organoids, a physiologically relevant model derived from different genetic backgrounds. Intestinal organoids were generated from both WT (Fig. 3 *A–E* and *SI Appendix*, Fig. S4 *A–D*) and *APC*$^{Min/+}$ mice (Fig. 3 *F–J* and *SI Appendix*, Fig. S4 *E–H*) and treated with 7-oxo-DCA, isoDCA, 3-oxo-DCA, DCA, along with their vehicle control (DMSO). Brightfield images captured the before and after treated organoids, with budding rates quantified as crypt domains per organoid. In both WT and *APC*$^{Min/+}$ organoids, we observed markedly increased budding and branching with 7-oxo-DCA, 3-oxo-DCA, and DCA treatments, but only a less significantly increased budding in isoDCA-treated organoids, compared to DMSO controls (Fig. 3 *A* and *F* and *SI Appendix*, Fig. S4 *A* and *E*). ATP production mirrored these trends, rising in 7-oxo-DCA, 3-oxo-DCA, and DCA-treated WT and *APC*$^{Min/+}$ organoids and declining in isoDCA-treated samples (Fig. 3 *B* and *G* and *SI Appendix*, Fig. S4 *B* and *F*). Further investigations involved

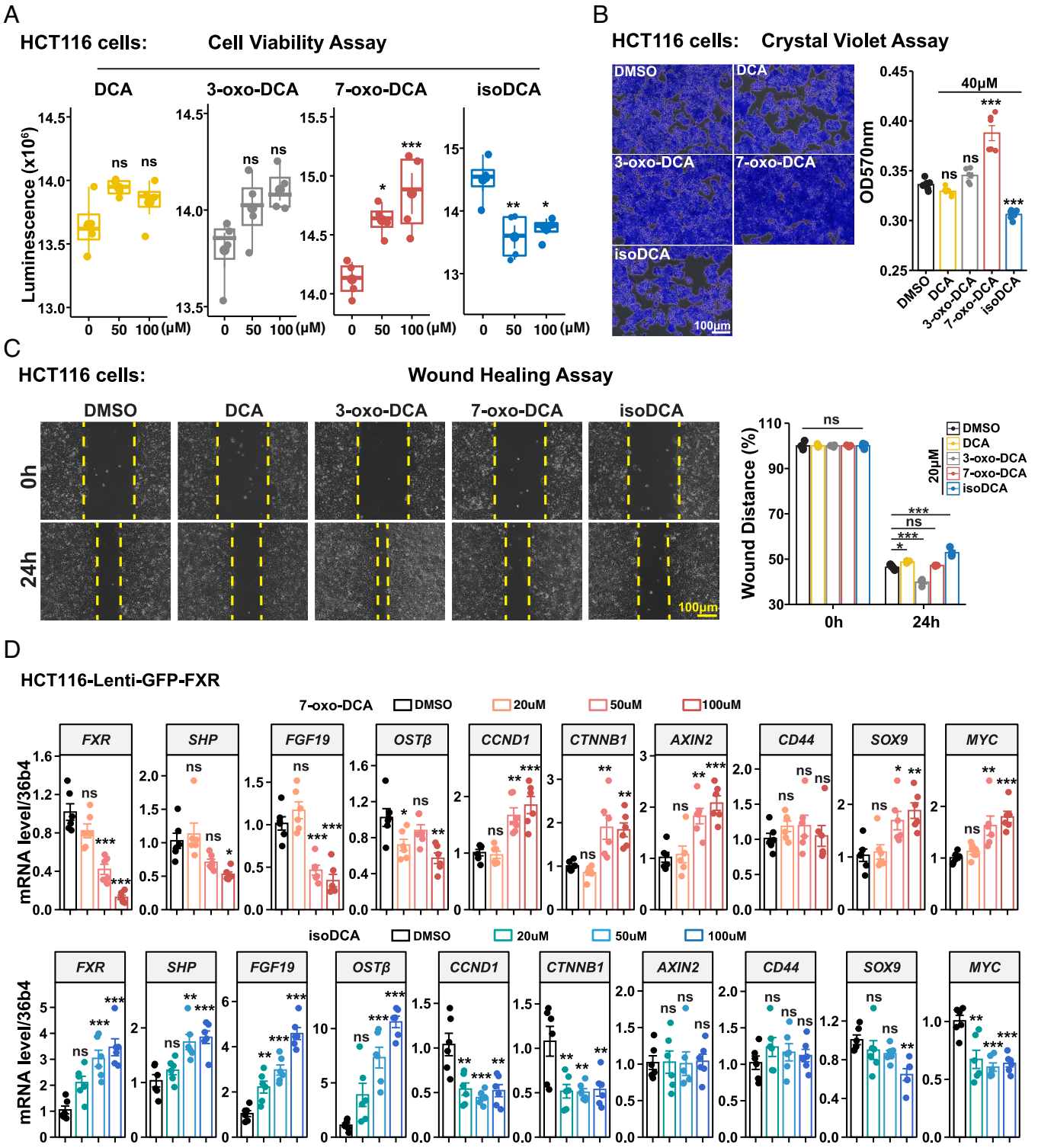

Fig. 2. 7-oxo-DCA promotes HCT116 cell growth while isoDCA suppresses it. (*A*) HCT116 cells were treated with increasing doses of DCA, 3-oxo-DCA, 7-oxo-DCA, and isoDCA for 24 h. Cell viabilities were measured by Celltiter-Glo kit. (*B*) HCT116 cells were treated with 40 μM of DCA, 3-oxo-DCA, 7-oxo-DCA, and isoDCA for 48 h. were measured by Crystal Violet stained cells and representative phase-contrast images were displayed, (Scale bar, 100 μm.) Quantitative data were measured as OD570nm readings. (*C*) HCT116 cells were treated with 20 μM of DCA, 3-oxo-DCA, 7-oxo-DCA, and isoDCA for 24 h. Representative images are shown and wound healing capabilities were quantified by the percentage of distances in between. (*D*) HCT116 cells with Lentivirus-mediated overexpressed FXR, were treated with dose-dependent (0, 20, 50, 100 μM) increase of 7-oxo-DCA and isoDCA for 24 h. The expression of *FXR* and its target genes (*SHP, FGF19, OSTβ*), cell cycling gene (*CCND1*), Wnt signaling gene (*CTNNB1, AXIN2, CD44*), and oncogenes (*SOX9, MYC*) were measured by RT-qPCR. All experiments were repeated three times independently, and representative data are shown as the mean ± SEM. For two-group comparison, Student's unpaired *t* tests were applied. For more than two group comparisons, the one-way ANOVA test followed by Tukey's or Dunn's multiple comparisons was applied. **P* < 0.05; ***P* < 0.01; ****P* < 0.005; ns: not significant.

costaining for the cell proliferation marker Ki67 and ISCs marker Olfm4 in BAs-treated WT and $APC^{Min/+}$ organoids. Increased Ki67 and Olfm4 staining was evident in budding crypts of 7-oxo-DCA, 3-oxo-DCA, and DCA-treated WT and $APC^{Min/+}$ organoids, while staining was reduced in isoDCA-treated organoids (Fig. 3 *C* and *H* and *SI Appendix*, Fig. S4 *C* and *G*). Additionally, expression

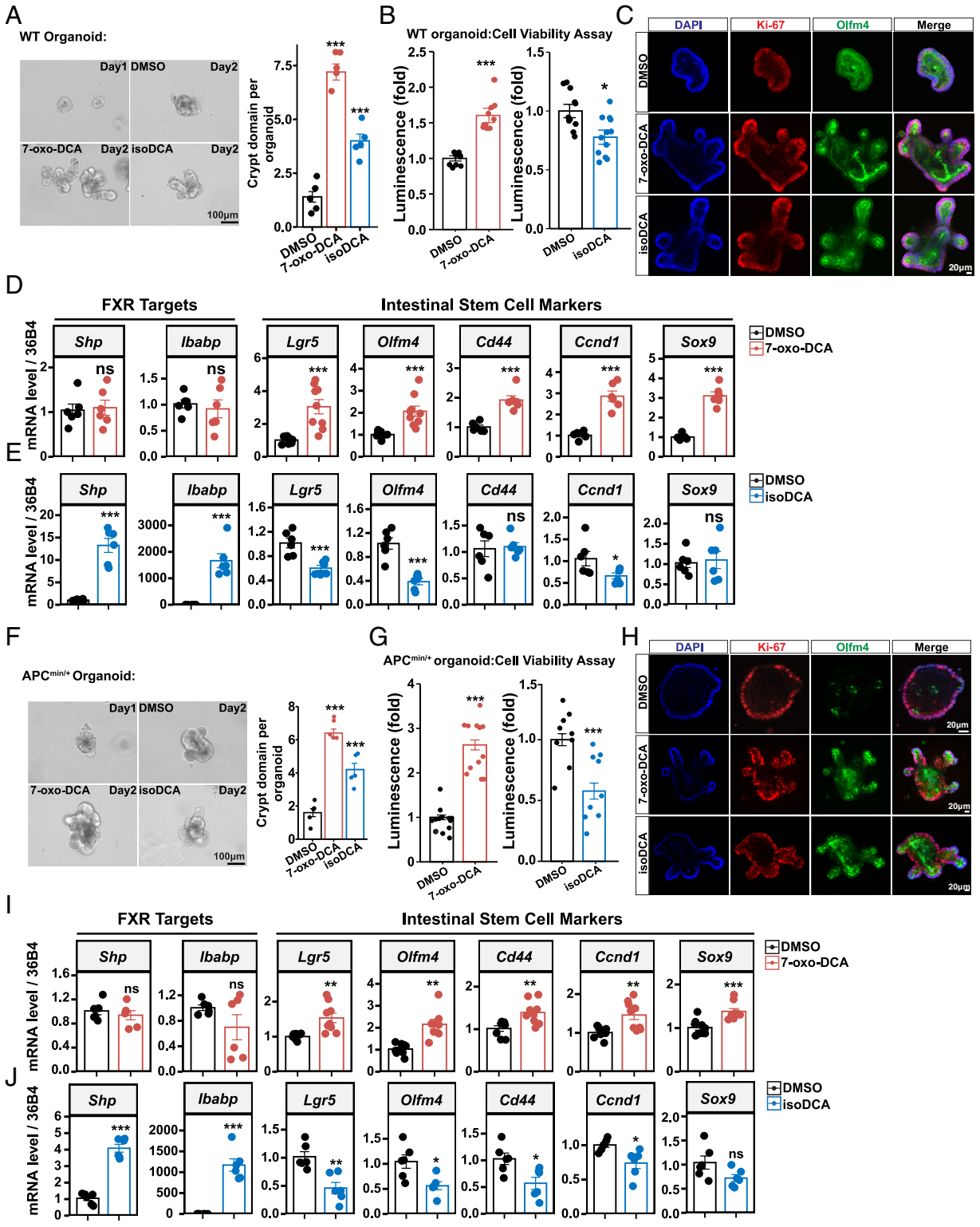

Fig. 3. 7-oxo-DCA stimulates ISC proliferation while isoDCA inhibits it in intestinal organoids. (*A*) WT organoids treated with 10 μM of 7-oxo-DCA and isoDCA with Vehicle (DMSO) on days 2 for 48 h. Brightfield images of organoids were presented, (Scale bar, 50 μm.) Proliferation rates were also quantified as crypt domain per organoids. (*B*) WT organoids were treated with 7-oxo-DCA, isoDCA, and DMSO for 24 h. Organoid viabilities were measured by Luminescent Celltiter-glo-3D kit. (*C*) Coimmunostaining images of ISCs marker Olfm4 (green) and proliferation gene marker Ki67 (red) in the WT organoids treated with 7-oxo-DCA, isoDCA, and DMSO for 48 h, (Scale bar, 20 μm.) (*D* and *E*) WT organoids were treated with 7-oxo-DCA, isoDCA, and DMSO for 24 h. Relative expressions of FXR target genes (*Shp*, *Ibabp*), ISC marker genes (*Lgr5*, *Olfm4*), and Wnt signaling genes (*Cd44*, *Ccnd1*, *Sox9*) were measured by RT-qPCR. (*F*) $APC^{Min/+}$ organoids treated with 10 μM of 7-oxo-DCA, isoDCA, and DMSO on days 2 for 48 h. Brightfield images of organoids were presented, (Scale bar, 50 μm.) *P*roliferation rates were also quantified as crypt domain per organoids. (*G*) $APC^{Min/+}$ organoids were treated with 7-oxo-DCA, isoDCA, and DMSO for 24 h. Organoid viabilities were measured by Luminescent Celltiter-glo-3D kit. (*H*) Coimmunostaining images of ISCs marker Olfm4 (green) and proliferation gene marker Ki67 (red) in the $APC^{Min/+}$ organoids treated with 7-oxo-DCA, isoDCA, and DMSO for 48 h, (Scale bar, 20 μm.) (*I* and *J*) $APC^{Min/+}$ organoids were treated with 7-oxo-DCA, isoDCA, and DMSO for 24 h. Relative expressions of FXR target genes (*Shp*, *Ibabp*), ISC marker genes (*Lgr5*, *Olfm4*), and Wnt signaling genes (*Cd44*, *Ccnd1*, *Sox9*) were measured by RT-qPCR. All experiments were repeated three times independently, and representative data are shown as the mean ± SEM. For two-group comparison, Student's unpaired *t* tests were applied. For more than two group comparisons, the one-way ANOVA test followed by Tukey's multiple comparisons was applied. **P* < 0.05; ***P* < 0.01; ****P* < 0.005; ns: not significant.

analysis of FXR target genes, ISCs signature genes, and Wnt signaling pathway genes revealed noteworthy findings in both WT and $APC^{Min/+}$ organoids treated with these microbial BAs. Notably, 7-oxo-DCA did not inhibit FXR target genes as a neutral antagonist, but isoDCA exhibited marked induction of FXR target genes as a potent agonist in both WT and $APC^{Min/+}$ organoids (Fig. 3 *D*, *E*, *I*, and *J*). One possible reason for 7-oxo-DCA fails to repress FXR target genes is that, as a neutral antagonist, 7-oxo-DCA may only exhibit inhibitory effects when counteracts with agonists. Nevertheless, we observed a significant increase in the expression of ISCs and Wnt signature genes upon 7-oxo-DCA, 3-oxo-DCA, and DCA treatment in both WT and $APC^{Min/+}$ organoids, and isoDCA conversely inhibited the expression of these genes. (Fig. 3 *D*, *E*, *I*, and *J* and *SI Appendix*, Fig. S4 *D* and *H*). To verify that the observed effects are channeled through the BA-FXR pathway, we carried out experiments on organoids derived from both WT and FXR knockout (FXRKO) mice, treating these organoids with 7-oxo-DCA and isoDCA. We found that the impacts of both BAs on FXR targets, ISC proliferation, and Wnt signaling genes were negated in FXRKO organoids, contrasting with the responses observed in WT organoids (*SI Appendix*, Fig. S4*I*). This suggests that the actions of 7-oxo-DCA and isoDCA are largely dependent on the presence of FXR in these processes. Additionally, we found that treatments of 7-oxo-DCA and isoDCA on colonic organoids consistently induced gene expression changes akin to those observed in small intestinal organoids (*SI Appendix*, Fig. S4*J*). Taken together, our findings unveil that 7-oxo-DCA bolsters the growth of WT and $APC^{Min/+}$ organoids by fostering ISCs' proliferation through FXR signaling downregulation. Conversely, isoDCA exerts opposing effects on ISCs' proliferation by strongly inducing FXR target genes.

7-oxo-DCA Enhances the Stemness in Patient-Derived Cancer Organoids (PDCOs) while isoDCA Impedes It. To assess the translational impact of 7-oxo-DCA and isoDCA, we employed PDCOs, which provide a more clinically relevant platform to investigate patient responses and better predict therapeutic outcomes (Fig. 4*A*). PDCOs were treated with 7-oxo-DCA, isoDCA, and their vehicle (DMSO) for 24 h, and the PDCOs viabilities were assessed by the ATP production. Consistent with the aforementioned mouse organoid findings, 7-oxo-DCA significantly promoted PDCOs' growth, while isoDCA curtailed it (Fig. 4*B*). Analyzing brightfield images of treated PDCOs over 0, 3, 6, and 9 d, we quantified organoids perimeter and area. Mirroring previous results, 7-oxo-DCA fostered PDCOs budding and growth compared to DMSO (Fig. 4 *C* and *D*). Intriguingly, isoDCA treatment did not hinder growth (Fig. 4 *C* and *D*); instead, isoDCA elevated PDCOs' size comparably to 7-oxo-DCA. Additionally, heightened costaining of the cell proliferation marker KI67 and ISCs marker LGR5 was observed in 7-oxo-DCA-treated PDCOs (Fig. 4 *E* and *F*). Inquisitively, despite isoDCA significantly increasing PDCOs' size, it notably reduced KI67 and LGR5 staining (Fig. 4 *E* and *F*). Further analysis encompassed FXR target genes, ISC, and Wnt signature genes in PDCOs exposed to 7-oxo-DCA and isoDCA on 24 h, 3, 6, and 9 d (Fig. 4 *G* and *H* and *SI Appendix*, Fig. S5). While 7-oxo-DCA did not substantially inhibit FXR target genes as a neutral antagonist, isoDCA strikingly induced these genes as a potent agonist (Fig. 4 *G* and *H*). Interestingly, isoDCA treatment robustly suppressed ISC and Wnt signaling genes, whereas 7-oxo-DCA considerably upregulated their expressions (Fig. 4 *G* and *H*). Collectively, 7-oxo-DCA and isoDCA exert opposing impacts on ISC and Wnt signature genes, yet both comparably propel PDCOs' growth. This discrepancy led us to investigate the PDCOs differentiation upon 7-oxo-DCA and isoDCA treatment. While 7-oxo-DCA did not significantly induce the expression of intestinal differentiated cell markers FABP2 and KRT20, isoDCA markedly elevated their expressions (Fig. 4 *G* and *H* and *SI Appendix*, Fig. S5). It is suggesting that isoDCA's augmentation of PDCOs' size might stem from its capacity to drive differentiation. These results underline the distinct effects of 7-oxo-DCA and isoDCA on PDCOs, underscoring their intricate roles in intestinal cell growth and cancer progression.

7-oxo-DCA Facilitates whereas isoDCA Inhibits the Intestinal Tumorigenesis In Vivo. Given that 7-oxo-DCA has been shown to promote, while isoDCA has demonstrated its ability to inhibit, cancer cell and organoid growth, we conducted in vivo experiments to further explore their effects on tumorigenesis. Initially, we performed in vivo EdU assays to access the cell proliferation rate in WT and $APC^{Min/+}$ mice. In WT mice, the administration of 7-oxo-DCA led to a noticeable increase in ISC proliferation (*SI Appendix*, Fig. S6*A*). Furthermore, in $APC^{Min/+}$ mice, we observed intensified EdU staining in adenomas, indicating an augmented cell proliferation response following 7-oxo-DCA administration (*SI Appendix*, Fig. S6*B*).

To investigate the potential of 7-oxo-DCA to promote and isoDCA to inhibit tumorigenesis in $APC^{Min/+}$ mice, we conducted a 5-wk gavage study, administering either 7-oxo-DCA, isoDCA, or their vehicle to the $APC^{Min/+}$ mice (Figs. 5*A* and 6*A*). Initially, intestinal permeability was evaluated by measuring plasma FITC-dextran levels. Notably, prolonged exposure to 7-oxo-DCA increased, while isoDCA decreased, intestinal permeability, as evidenced by altered FITC-dextran levels in the plasma (Figs. 5*B* and 6*B*). Moreover, we observed total plasma BAs are elevated upon 7-oxo-DCA and a trend to decline upon isoDCA, hinting at a potential link between microbial BAs and changes in intestinal barrier function (Figs. 5*C* and 6*C*). Strikingly, our findings revealed a significant rise in tumor numbers in both the small intestine and colon of $APC^{Min/+}$ mice upon 7-oxo-DCA administration (Fig. 5 *D*–*G*), while isoDCA treatment led to a notable reduction in tumor loads (Fig. 6 *D*–*G* and *SI Appendix*, Fig. S6*C*). H&E staining further highlighted greater hyperplasia in adenomas within the 7-oxo-DCA group (Fig. 5*H*), but decreased proliferation in the isoDCA group (Fig. 6*H*). In addition, Alcian-Blue staining showed that the secretive cells were notably reduced in the 7-oxo-DCA-treated group across both small intestine and colon segments, indicating potential disruptions in cell differentiation (*SI Appendix*, Fig. S6*D*). Notably, immunostaining for the cell proliferation marker Ki67 and the cell cycling marker Ccnd1 revealed a significant increase in proliferating cell populations within adenomas of both small intestine and colon segments in the 7-oxo-DCA group (Fig. 5 *I* and *J* and *SI Appendix*, Fig. S6 *E* and *F*), but a remarkable decline in the isoDCA group (Fig. 6 *I* and *J*). Moreover, an accumulation of β-catenin protein suggesting enhanced activation of the Wnt signaling pathway, was observed in 7-oxo-DCA-treated mice but not in the isoDCA-treated ones (Figs. 5*I* and 6*I* and *SI Appendix*, Fig. S6*E*). Interestingly, Keratin 20 (Krt20) expression was not detected within the adenoma but showed increased presence adjacent to the adenoma in the 7-oxo-DCA treatment group but reduced in the isoDCA group (Figs. 5*I* and 6*I* and *SI Appendix*, Fig. S6*E*). These histological features align with the adenoma to adenocarcinoma transition, further supporting the role of 7-oxo-DCA in driving tumorigenesis and malignant transformation in $APC^{Min/+}$ mice, whereas isoDCA could effectively reverse these progressions.

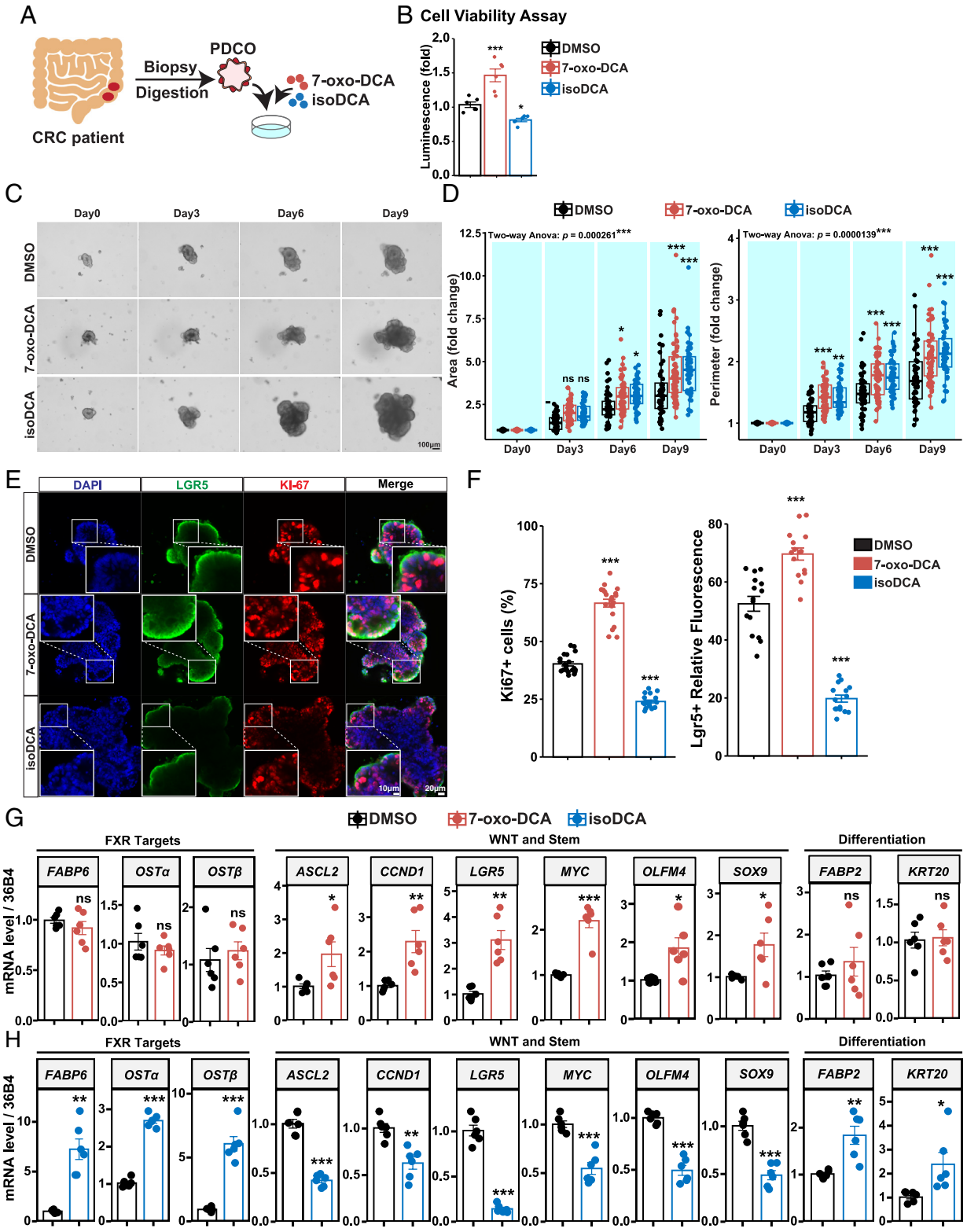

Fig. 4. 7-oxo-DCA enhances the stemness in PDCOs, while isoDCA impedes it. (*A*) Schematic of human CRC PDCOs isolation from human patients, then subjected to 7-oxo-DCA and isoDCA experiments. (*B*) PDCOs were treated with 20 μM of 7-oxo-DCA and isoDCA with DMSO for 24 h. Organoid viabilities were measured by Celltiter-glo-3D kit. (*C* and *D*) PDCOs were treated with 20 μM of 7-oxo-DCA and isoDCA with DMSO for 9 d, (Scale bar, 20 μm.) Brightfield images were taken at day 0, 3, 6, 9. The area and perimeter were quantified (*D*). (*E* and *F*) Coimmunostaining of ISCs marker LGR5 (green) and proliferation gene marker Ki67 (red). PDCOs were treated with 20 μM of 7-oxo-DCA and isoDCA with DMSO for 9 d, (Scale bar, 20 μm.) KI67 positive cells and LGR5 mean fluorescence intensity (MFI) were quantified (*F*). (*G* and *H*) PDCOs were treated with 20 μM of 7-oxo-DCA (24 h) and isoDCA (9 d); relative expressions of FXR target genes (*FABP6, OSTα, OSTβ*), ISC, and Wnt signature genes (*ASCL2, CCND1, LGR5, MYC, OLFM4,* and *SOX9*) were measured by RT-qPCR. Experiments were independently replicated twice, and representative data are shown as the mean ± SEM. For two group comparison, Student's unpaired *t* test were applied. For more than two group comparisons, one-way ANOVA or two-way ANOVA tests followed by Tukey's multiple comparisons were applied. **P* < 0.05; ***P* < 0.01; ****P* < 0.005; ns: not significant.

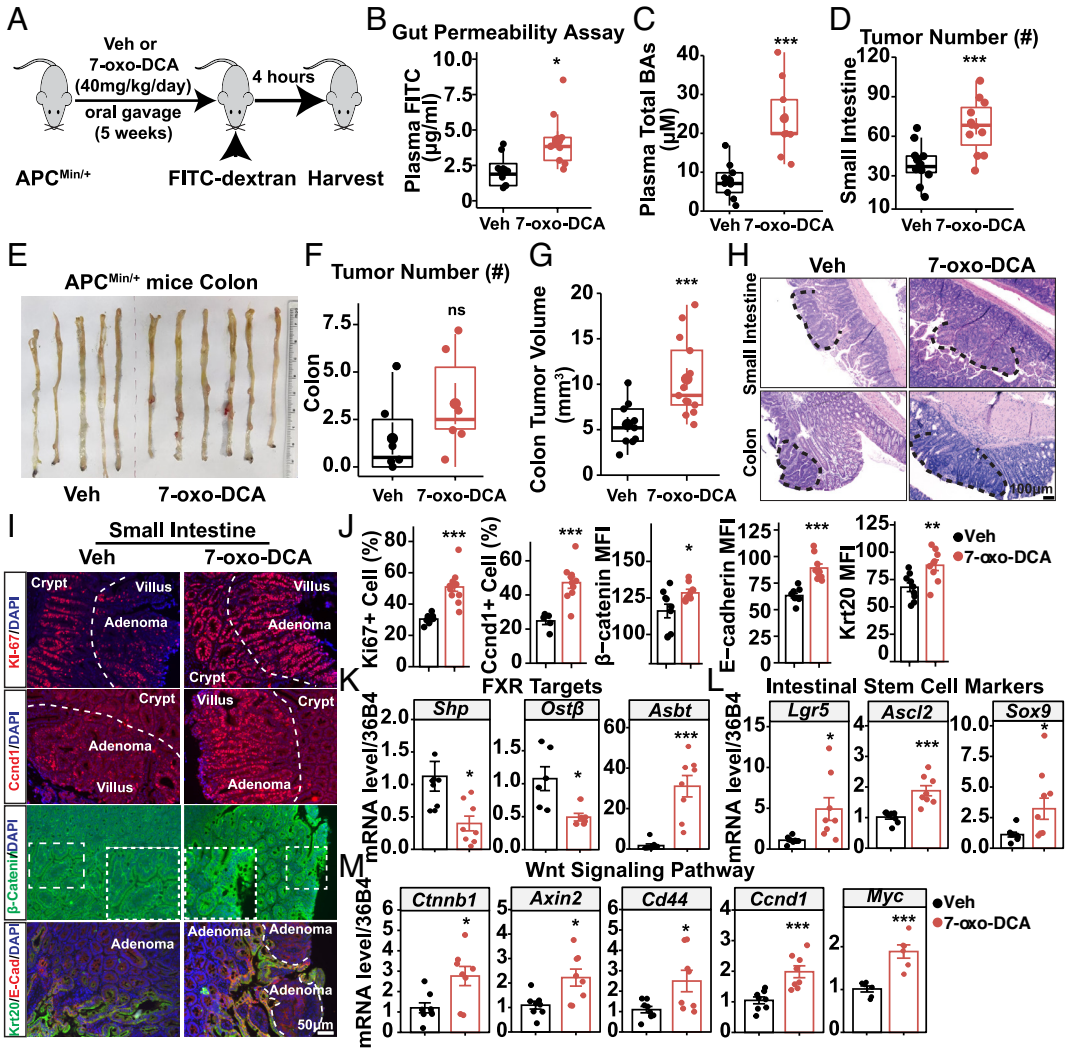

Fig. 5. 7-oxo-DCA enhances tumorigenesis in $APC^{Min/+}$ mice. (*A*) Schematics of 7-oxo-DCA (40 mg/kg BW p.o.) or vehicle (corn oil) were administrated in $APC^{Min/+}$ mice for 5 wk. (*B*) Intestinal permeability measured after 4 h of FITC-dextran administration in both 7-oxo-DCA and vehicle-treated $APC^{min/+}$ mice. (*C*) Total BAs were measured in the plasma of 7-oxo-DCA and vehicle-treated groups. (*D*) Total tumor numbers in small intestine segment. (*E–G*) Colon image (*E*), colon tumor number (*F*), and volume (*G*) of mice in the above treatment groups. (*H*) Representative H&E staining of small intestine and colon segments of $APC^{Min/+}$ mice in the above treatment groups, with large tumors outlined. (Scale bar, 100 μm.) (*I* and *J*) Immunostaining of differentiated intestinal tumor marker cytokeratin 20 (Krt20, green), Epithelial-specific adhesion molecule E-cadherin (E-cad, red); Proliferation gene marker Ki67 (red), Cell cycle gene Ccnd1 (red), Wnt pathway signature protein β-catenin (green) in the small intestine of $APC^{Min/+}$, with large tumors outlined (*I*). Quantification of Ki67 positive cells, Ccnd1 positive cells, MFI of β-Catenin, E-Cadherin, and Krt20 displayed in images (*J*). (Scale bar, 50 μm.) (*K–M*) Relative expression of FXR targets (*K*), ISC genes (*Lgr5, Ascl2, Sox9*) (*L*) and Wnt signaling genes (*Ctnnb1, Axin2, Cd44, Ccnd1*) (*M*) in $APC^{Min/+}$ mice in the above treatment groups, measured by RT-qPCR. n = 8-10/group. Experiments were independently replicated twice, and representative data are shown as the mean ± SEM. For two group comparison, Student's unpaired *t* test were applied. For more than two group comparison, the one-way ANOVA test was followed by multiple comparisons. $*P < 0.05$; $**P < 0.01$; $***P < 0.005$; ns: not significant

To corroborate our hypothesis at the gene level, we examined the expression of FXR target genes, lSCs, and Wnt signaling genes in $APC^{Min/+}$ mice with 7-oxo-DCA or isoDCA treatment. Surprisingly, following 5 wk of 7-oxo-DCA administration in vivo, we observed a suppression of FXR target genes (Fig. 5*K*), suggesting its potential role as an antagonist countering other endogenous agonistic BAs within the in vivo setting. As expected, we also noted a profound activation of FXR targets upon isoDCA treatment in vivo (Fig. 6*K*). Moreover, we observed a significant upregulation in ISC gene expression (Fig. 5*L*) and Wnt signaling genes (Fig. 5*M*) in 7-oxo-DCA group, but a remarkable downregulation of those genes in the isoDCA group (Fig. 6 *L* and *M*), aligning with their effects observed in organoids. Additionally, the potential induction of TGFβ signaling by 7-oxo-DCA in vivo (*SI Appendix*, Fig. S6*G*), implying its capacity to advance tumor progression.

To validate whether 7-oxo-DCA and isoDCA could directly affect Wnt activities, we performed Wnt luciferase reporter assay in vitro. In agreement with the gene expression results, 7-oxo-DCA heightened the Wnt pathway activities, and isoDCA inhibited them (*SI Appendix*, Fig. S7*A*). To further elucidate whether their impact on Wnt signaling is FXR-dependent, we employed FXR-specific siRNA to reduce FXR expression in cells, and then assessed the effects of 7-oxo-DCA and isoDCA on these cells. Significantly, Wnt luciferase activities were markedly increased following the knockdown of FXR (*SI Appendix*, Fig. S7 *B* and *C*).

7-oxo-DCA and isoDCA Reshape the BAs Pool and Gut Microbiome in $APC^{Min/+}$ Mice. Given the opposing effects of 7-oxo-DCA and isoDCA on tumorigenesis, we propose that they might also influence the tumor microenvironment, including metabolite pools and the gut microbiome. Initially, we explored alterations in the BAs pool. We observed that isoDCA significantly reduced primary BAs and increased secondary BAs in the plasma, while it decreased secondary BAs and increased primary BAs in the cecum, revealing that isoDCA potentially increased BA diversity in the host (Fig. 7*A*). In contrast, 7-oxo-DCA did not change the BAs

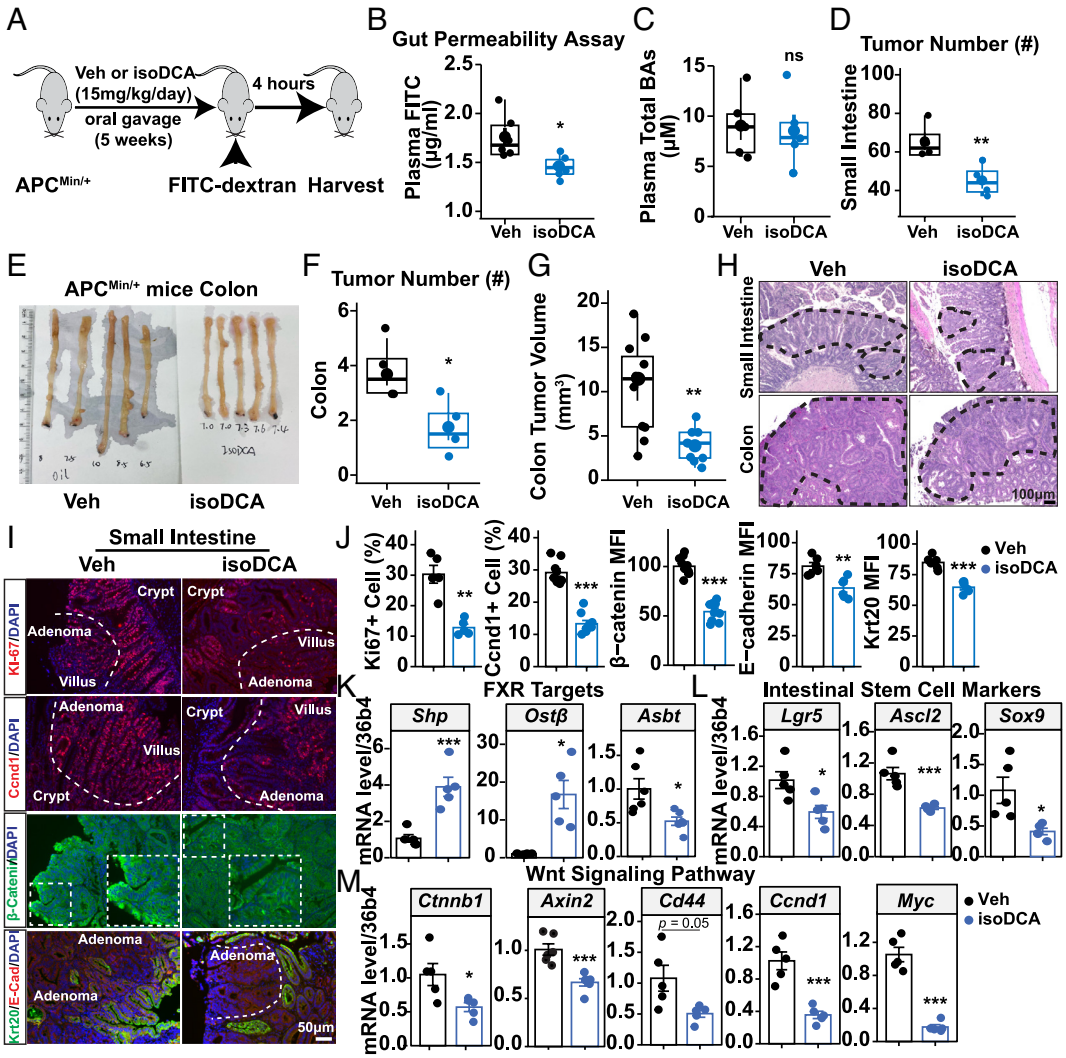

Fig. 6. isoDCA inhibits tumorigenesis in *APC*$^{Min/+}$ mice. (*A*) Schematics of isoDCA (15 mg/kg BW p.o.) or vehicle (corn oil) were administrated in *APC*$^{Min/+}$ mice for 5 wk. (*B*) Intestinal permeability measured after 4 h of FITC-dextran administration in both isoDCA and vehicle-treated *APC*$^{Min/+}$ mice. (*C*) Total BAs were measured in the plasma of 7-oxo-DCA and vehicle-treated groups. (*D*) Total tumor numbers in small intestine segment. (*E–G*) Colon image (*E*), colon tumor number (*F*), and volume (*G*) of mice in the above treatment groups. (*H*) Representative H&E staining of small intestine and colon segments of *APC*$^{Min/+}$ mice in the above treatment groups, with large tumors outlined. (Scale bar, 100 μm.) (*I* and *J*) Immunostaining of differentiated intestinal tumor marker cytokeratin 20 (Krt20, green), Epithelial-specific adhesion molecule E-cadherin (E-cad, red); Proliferation gene marker Ki67 (red), Cell cycle gene Ccnd1 (red), Wnt pathway signature protein β-catenin (green) in the small intestine of *APC*$^{Min/+}$, with large tumors outlined (*I*). Quantification of Ki67 positive cells, Ccnd1 positive cells, MFI of β-Catenin, E-Cadherin, and Krt20 displayed in images (*J*). (Scale bar, 50 μm.) (*K–M*) Relative expression of FXR targets (*K*), ISC genes (*Lgr5, Ascl2, Sox9*) (*L*) and Wnt signaling genes (*Ctnnb1, Axin2, Cd44, Ccnd1*) (*M*) in *APC*$^{Min/+}$ mice in the above treatment groups, measured by RT-qPCR. n = 5-8/group. Experiments were independently replicated twice, and representative data are shown as the mean ± SEM. For two group comparison, Student's unpaired *t* test were applied. For more than two group comparison, the one-way ANOVA test was followed by multiple comparisons. *$P < 0.05$; **$P < 0.01$; ***$P < 0.005$; ns: not significant

pool in the plasma but significantly reduced primary BAs in the cecum, showing an effect opposite to that of isoDCA (Fig. 7*A*). Additionally, we detected an increase in unconjugated BAs and a decrease in conjugated ones in both plasma and cecum samples in the isoDCA-treated group, suggesting that isoDCA may decrease gut permeability by altering the conjugated/unconjugated ratio (Fig. 7*B*). Specifically, we noted that 7-oxo-DCA significantly elevated levels of CA, T-CA, G-CA, βMCA, T-βMCA, and DCA in the plasma (Fig. 7*C*), and its administration was confirmed by the increased presence of 7-oxo-DCA itself in the cecum (Fig. 7*C*). Intriguingly, isoDCA treatment resulted in decreased levels of CA, CDCA, and DCA in the plasma, suggesting a potential reduction in the total amount of BAs (Fig. 7*D*). Notably, isoDCA broadly reduced both primary and secondary BAs in the cecum, including T-βMCA, DCA, and 7-oxo-DCA, with the exception of a significant increase in UDCA, LCA, and isoalloLCA (*SI Appendix*, Fig. S8 *A* and *B*). This implies that isoDCA might favor microbial activity involved in converting CDCA to UDCA, LCA, and their derivatives. Intriguingly, isoDCA levels were found to be very low in both plasma and cecum samples (Fig. 7*D* and *SI Appendix*, Fig. S8*B*), with relative levels confirming its in vivo administration. This suggests a potentially high conversion rate of isoDCA by gut microbes.

To investigate the impact of 7-oxo-DCA and isoDCA on gut microbiome during CRC progression, we analyzed its changes by conducting 16S rRNA sequencing of cecum samples from groups treated with 7-oxo-DCA, isoDCA, and a vehicle control. The bacterial diversity and composition were assessed using both alpha and beta diversity metrics (Fig. 7*E*). The Shannon Index for alpha diversity indicated a significant reduction in microbial diversity following 7-oxo-DCA treatment compared to the vehicle, while isoDCA showed a tendency to increase diversity (Fig. 7*F*). Beta diversity differences were also notable on PCoA plots derived from Bray–Curtis dissimilarity and Unweighted UniFrac distance, revealing that both 7-oxo-DCA and isoDCA treatments distinctly modified gut microbiota composition relative to the vehicle control (Fig. 7*F*

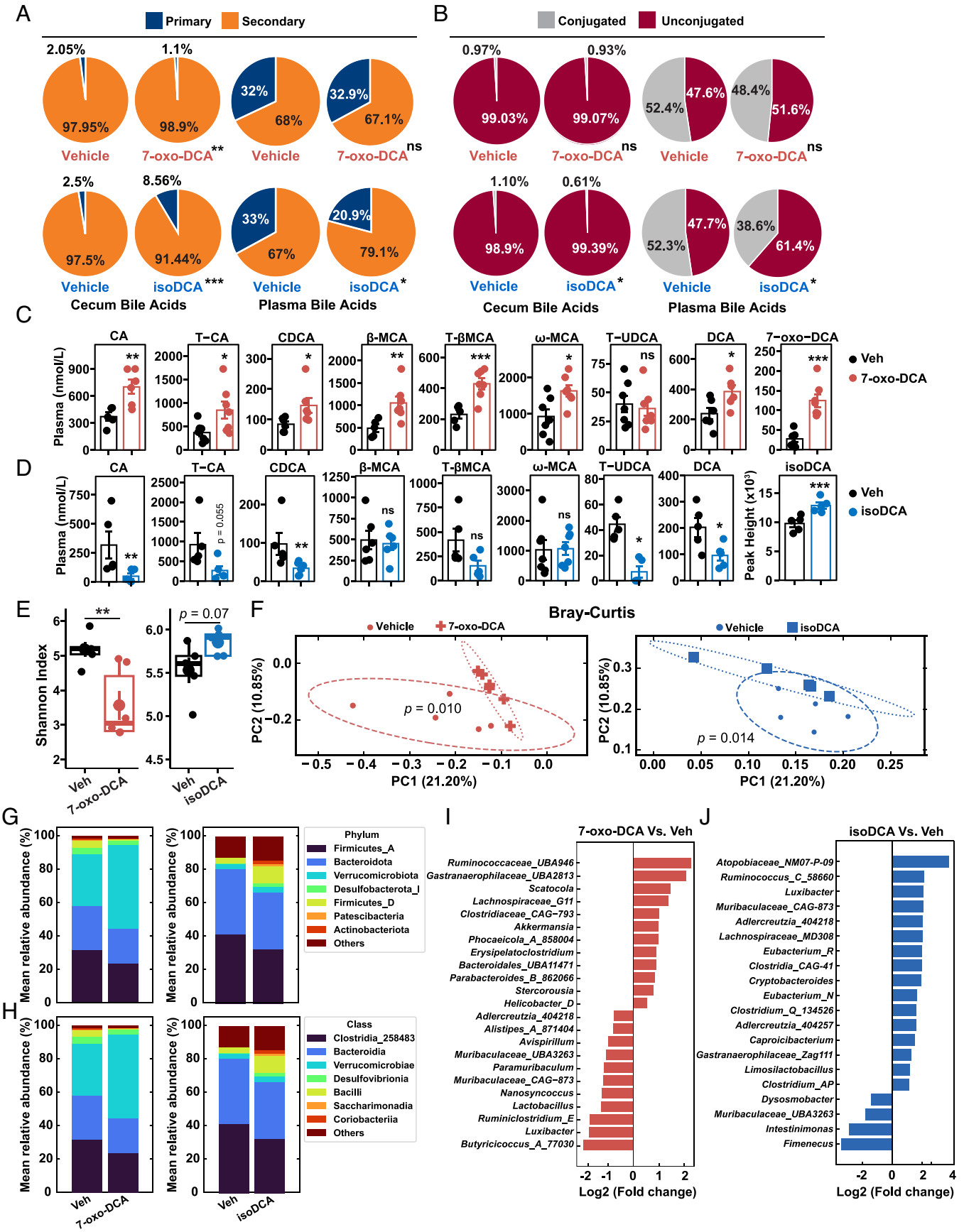

Fig. 7. 7-oxo-DCA and isoDCA reshape the BAs pool and gut microbiome in *APC*$^{Min/+}$ mice. (*A*) Cecum and plasma primary and secondary BAs composition in Veh-, 7-oxo-DCA-, and isoDCA-treated *APC*$^{Min/+}$ mice. (*B*) Cecum and plasma conjugated and unconjugated BAs composition in Veh-, 7-oxo-DCA-, and isoDCA-treated *APC*$^{Min/+}$ mice. (*C* and *D*) Plasma individual BAs were measured in Vehicle, 7-oxo-DCA (*C*), and isoDCA (*D*) treated *APC*$^{Min/+}$ mice. (*E*) Alpha diversity of *APC*$^{Min/+}$ mice gavaged with 7-oxo-DCA and isoDCA. (*F*) Beta diversity of *APC*$^{Min/+}$ mice gavaged with 7-oxo-DCA and isoDCA. (*G* and *H*) Taxonomy at the Phylum level (*G*) and Class level (*F*) of Veh-, 7-oxo-DCA-, and isoDCA-treated *APC*$^{Min/+}$ mice. (*I* and *J*) Differential abundance at the genus level in 7-oxo-DCA vs. Vehicle (*I*) and isoDCA vs. Vehicle (*J*) group.

and *SI Appendix*, Fig. S8*E*). Further examination of specific microbial taxa revealed that 7-oxo-DCA treatment slightly increased Bacteroidota and decreased Clostridia at the phylum and class levels, respectively (Fig. 7 *G* and *H*). In contrast, isoDCA treatment seemed to decrease the abundance of Bacteroidota while increasing that of *Verrucomicrobiota* and *Desulfovibrionia* compared to the vehicle (Fig. 7 *G* and *H*). Specifically, we observed that 7-oxo-DCA elevated levels of *Ruminococcus_UBA946* and *Helicobacter_D*, both of which have been associated with intestinal tumorigenesis and inflammation (Fig. 7*I*). Conversely, it reduced levels of *Lactobacillus Ruminiclostridium_E* and *Butyricicoccus_A_77030*, which are known for their anti-inflammatory and butyrate-producing properties (Fig. 7*I*). 7-oxo-DCA also increased levels of *Akkermansia muciniphila*, an overabundance of which could excessively thin the mucus layer, potentially exposing the gut epithelium to carcinogenic compounds or pathogens that promote cancer due to its mucin-degrading properties (Fig. 7*I*). However, *Akkermansia*'s role in CRC remains controversial, and its specific response to 7-oxo-DCA requires further investigation. In contrast, isoDCA induced an increase in several strains, including *Ruminococcus_C_58660*, *Lachnospiraceae_MD308*, *Caproicibacterium*, *Limosilactobacillus*, and *Muribaculaceae_CAG-873* (Fig. 7*J*). These are generally short-chain fatty acids (SCFAs) producers, which can decrease CRC due to their anti-inflammatory and tumor-suppressing roles. Intriguingly, isoDCA increased the abundance of more bacterial species while reducing fewer, potentially due to its ability to enhance overall abundance and diversity (Fig. 7*J*). Notably, isoDCA and 7-oxo-DCA showed opposing effects on *Adlercreutzia* and *Luxibacter* strains (Fig. 7 *I* and *J*). Specifically, isoDCA treatment increased the abundance of SCFA-producing genera such as *Amulumruptor*, *Roseburia_1XD42-69*, *Lachnoclostridium_B*, contrasting with 7-oxo-DCA, which elevated *Helicobacter_D* and *Prevotella_CAG-873* strains potentially linked to gut inflammation and CRC progression (*SI Appendix*, Fig. S8*E*). Interestingly, isoDCA significantly increased the abundance of *Akkermansia* compared to 7-oxo-DCA, suggesting differing mechanisms of action of *Akkermansia* in the two treatments (*SI Appendix*, Fig. S8*E*). Remarkably, 7-oxo-DCA also increased *Phocaeicola vulgatus (Phocaeicola_A_858004)*, which has bile salt hydrolase (BSH) activity, indicating differences in BAs metabolism between the treatments with 7-oxo-DCA and isoDCA (*SI Appendix*, Fig. S8*E*).

In summary, these findings shed light on the tumorigenic properties of 7-oxo-DCA and antitumorigenic potentials of isoDCA in IECs and underscore the intricate regulatory networks involving microbial BAs and the FXR signaling pathway in influencing gut microbiome and gut health.

Discussion

CRC stands as one of the prevalent primary tumors globally, marked by escalating morbidity and mortality rates (1). A mounting body of evidence underlines the link between CRC and alterations in gut microbiota abundance, composition, and barrier function, all intertwined with the influence of metabolites shaped and altered by gut microbes (1, 2). This research unveiled certain microbiome-modulated BAs, such as 7-oxo-DCA and isoDCA, whose dynamics shift during tumorigenesis. Their effects on IECs and their potential role in driving CRC progression were explored in this study.

The gut microbiome performs numerous transformations on BAs, pivotal for lipid digestion and nutrient signaling (1). Primary BAs like cholic acid (CA) and CDCA, derived from cholesterol via the enzyme CYP7A1, are converted by gut bacteria into more hydrophobic secondary BAs such as DCA and LCA (28, 30, 33). Moreover, specific gut microbes are capable of converting more hydrophobic oxo-BAs into hydrophilic iso-BAs. Notably, these microorganisms, responsible for oxidation and epimerization of the 3-, 7-, and 12-hydroxy groups of BAs, encompass similar yet diverse hydroxysteroid dehydrogenase (HSDH) capabilities (28, 30, 33). Intriguingly, the gut also hosts aldo-keto reductase 1b7 (Akr1b7), an enzyme capable of catalyzing the conversion of 3-oxo-BAs to 3-epi-BAs, a process that can be enhanced through FXR activation (34). Whether governed by the gut microbiota or the host, the proposition that isoDCA exhibits hydrophilic attributes, potentially rendering it less toxic than 7-oxo-DCA, holds merit.

Many bacteria, including *Bacteroides*, *Clostridium*, and *Ruminococcus*, harbor 7α/β-HSDH enzymes crucial for BA modification, driven by BA-inducible (bai) operons (28, 30, 33). Dietary influences, such as a HFD, can increase the prevalence of BA-altering bacteria, suggesting a diet-microbiota link to cancer risk (31, 32). While the specific microbes responsible for converting 7-oxo-DCA to isoDCA remain unidentified, they likely act on CA as a common precursor, indicating a competitive substrate interaction within the gut ecosystem.

Nonetheless, it's worth noting that 7-oxo-DCA and isoDCA could serve as a potential biomarker for the initiation and progression of intestinal tumors. As mentioned earlier, plasma levels of 7-oxo-DCA exhibited the most robust correlations with advanced stages of hepatic fibrosis, NASH, and ballooning (26). Furthermore, there were nominal associations between genetic variants at various NAFLD/NASH loci and elevated levels of 7-oxo-DCA (26). Investigating the metabolomics and HMP2 cohorts from various IBD patients also showed a progressive increase in 7-oxo-DCA levels and a decrease in isoDCA levels during the course of the disease (18).

In addition to their distinct hydrophobicity features, our study has unveiled the significant biological implications of 7-oxo-DCA and isoDCA. Specifically, we established that 7-oxo-DCA functions as a neutral FXR antagonist, driving intestinal tumorigenesis, while isoDCA acts as a potent FXR agonist, inhibiting intestinal tumorigenesis. This insight was validated not only in a CRC mice model, but also through experimentation on primary mouse intestinal organoids, along with human cancer cell lines and PDCOs. Mechanistically, we uncovered that 7-oxo-DCA propels ISCs' proliferation by activating the Wnt signaling pathway, whereas isoDCA curbs ISCs' growth by repressing Wnt signaling, with both effects dependent on their interaction with FXR. It is important to note that the concentrations of 7-oxo-DCA and isoDCA used in some in vitro experiments significantly exceed their IC50 (13.8 μM) and EC50 (4.4 μM) values, potentially reaching supraphysiological levels. Therefore, additional research is essential to comprehensively understand the physiological roles of these BAs under normal conditions. Together, these groundbreaking findings highlight the tumorigenic properties of 7-oxo-DCA and the antitumorigenic potential of isoDCA in IECs, underscoring the complex regulatory networks involving microbial BAs and the FXR signaling pathway (*SI Appendix*, Fig. S7*D*). Significantly, our results highlight that isoDCA emerges as a notably stronger agonist for FXR, exceeding CDCA in potency in our studies. This observation holds implications for future endeavors in designing FXR-related therapeutics for CRC.

Materials and Methods

In this study, we employed a comprehensive set of experimental techniques to investigate the effects of BAs on intestinal health and cancer progression. Animal models and human PDCOs were utilized to assess the impact of BAs on

tumorigenesis and intestinal barrier function. Experimental methods included total BAs measurements, EdU incorporation experiments in vivo. Additionally, cell viability, luciferase assays, and various staining methods such as Hematoxylin & Eosin, Alcian Blue, and immunofluorescence staining were applied to evaluate cellular and tissue responses. Gene expression analysis, untargeted metabolomics of cecum samples, and targeted LC-MS for cecum and serum BA, and microbiome sequencing further complemented our investigative approaches, providing a detailed understanding of the host and microbial interactions. All methods are elaborated in *SI Appendix, Materials and Methods* section of our paper.

Data, Materials, and Software Availability. All study data are included in the article and/or *SI Appendix*.

ACKNOWLEDGMENTS. We would like to express our sincere gratitude to Dr. Ronald Evans at Salk Institute for generously providing us with the FXRKO mice. This work is funded by University of Wisconsin–Madison startup grants (AAI3795, AAI3894), University of Wisconsin Carbone Cancer Center startup support (AAI5122), University of Wisconsin fall competition support from Wisconsin Alumni Research Foundation (AAL8735), Badger Challenge award (AAM7958), PhRMA foundation Faculty Starter Grant (2024-FSGDS-1161699), American Cancer Society Coaches vs. Cancer Bo Ryan-Jay Holliday Families Fund Research Scholar Grant (RSG-23-1150338-01), Margaret Q. Landenberger Research Foundation (AAM7699), and NIH 1R37CA288447-01 to T.F.

Author affiliations: [a]Pharmaceutical Sciences Division, School of Pharmacy, University of Wisconsin–Madison, Madison, WI 53705; [b]School of Life Science, Arizona State University, Tempe, AZ 85287; [c]Department of Chemistry, University of British Columbia, Vancouver, BC V6T 1Z1, Canada; [d]Division of Hematology and Oncology, Department of Medicine, University of Wisconsin–Madison, Madison, WI 53705; [e]McArdle Laboratory for Cancer Research, Department of Oncology, University of Wisconsin–Madison, Madison, WI 53705; and [f]School of Medicine and Public Health, University of Wisconsin Carbone Cancer Center, Madison, WI 53792

1. C. L. Sears, W. S. Garrett, Microbes, microbiota, and colon cancer. *Cell Host Microbe* **15**, 317–328 (2014).
2. C. Degirolamo, S. Modica, G. Palasciano, A. Moschetta, Bile acids and colon cancer: Solving the puzzle with nuclear receptors. *Trends Mol. Med.* **17**, 564–572 (2011).
3. J. R. Walters, Bile acid diarrhoea and FGF19: New views on diagnosis, pathogenesis and therapy. *Nat. Rev. Gastroenterol. Hepatol.* **11**, 426–434 (2014).
4. O. Chavez-Talavera, A. Tailleux, P. Lefebvre, B. Staels, Bile acid control of metabolism and inflammation in obesity, type 2 diabetes, dyslipidemia, and nonalcoholic fatty liver disease. *Gastroenterology* **152**, 1679–1694.e3 (2017).
5. C. B. Ferrebee *et al.*, Organic solute transporter alpha-beta protects ileal enterocytes from bile acid-induced injury. *Cell Mol. Gastroenterol. Hepatol.* **5**, 499–522 (2018).
6. S. A. Kliewer, D. J. Mangelsdorf, Bile acids as hormones: The FXR-FGF15/19 pathway. *Dig. Dis.* **33**, 327–331 (2015).
7. C. D. Fuchs, M. Trauner, Role of bile acids and their receptors in gastrointestinal and hepatic pathophysiology. *Nat. Rev. Gastroenterol. Hepatol.* **19**, 432–450 (2022).
8. T. Fu *et al.*, FXR regulates intestinal cancer stem cell proliferation. *Cell* **176**, 1098–1112.e18 (2019).
9. Y. C. Kim *et al.*, Transgenic mice lacking FGF15/19-SHP phosphorylation display altered bile acids and gut bacteria, promoting nonalcoholic fatty liver disease. *J. Biol. Chem.* **299**, 104946 (2023).
10. T. Fu *et al.*, Paired microbiome and metabolome analyses associate bile acid changes with colorectal cancer progression. *Cell Rep.* **42**, 112997 (2023).
11. J. C. W. de Jong, N. Ijssennagger, S. W. C. van Mil, Breast milk nutrients driving intestinal epithelial layer maturation via Wnt and Notch signaling: Implications for necrotizing enterocolitis. *Biochim. Biophys. Acta Mol. Basis Dis.* **1867**, 166229 (2021).
12. J. H. Kemis *et al.*, Genetic determinants of gut microbiota composition and bile acid profiles in mice. *PLoS Genet.* **15**, e1008073 (2019).
13. P. Xu *et al.*, Intestinal sulfation is essential to protect against colitis and colonic carcinogenesis. *Gastroenterology* **161**, 271–286.e11 (2021).
14. H. Li *et al.*, Integrative systems analysis identifies genetic and dietary modulators of bile acid homeostasis. *Cell Metab.* **34**, 1594–1610.e4 (2022).
15. G. Sorrentino *et al.*, Bile acids signal via TGR5 to activate intestinal stem cells and epithelial regeneration. *Gastroenterology* **159**, 956–968.e8 (2020).
16. S. I. Sayin *et al.*, Gut microbiota regulates bile acid metabolism by reducing the levels of tauro-beta-muricholic acid, a naturally occurring FXR antagonist. *Cell Metab.* **17**, 225–235 (2013).
17. X. Dong, C. Cai, T. Fu, FXR suppresses colorectal cancer by inhibiting the Wnt/beta-catenin pathway via activation of TLE3. *Genes Dis.* **10**, 719–722 (2023).
18. D. Paik *et al.*, Human gut bacteria produce Tau(Eta)17-modulating bile acid metabolites. *Nature* **603**, 907–912 (2022).
19. S. Hang *et al.*, Bile acid metabolites control T(H)17 and T(reg) cell differentiation. *Nature* **576**, 143–148 (2019).
20. C. Campbell *et al.*, Bacterial metabolism of bile acids promotes generation of peripheral regulatory T cells. *Nature* **581**, 475–479 (2020).
21. T. Fu *et al.*, FXR mediates ILC-intrinsic responses to intestinal inflammation. *Proc. Natl. Acad. Sci. U.S.A.* **119**, e2213041119 (2022).
22. M. L. Chen *et al.*, CAR directs T cell adaptation to bile acids in the small intestine. *Nature* **593**, 147–151 (2021).
23. Y. Sato *et al.*, Novel bile acid biosynthetic pathways are enriched in the microbiome of centenarians. *Nature* **599**, 458–464 (2021).
24. M. Arifuzzaman *et al.*, Inulin fibre promotes microbiota-derived bile acids and type 2 inflammation. *Nature* **611**, 578–584 (2022).
25. G. Xie *et al.*, Sex-dependent effects on gut microbiota regulate hepatic carcinogenic outcomes. *Sci. Rep.* **7**, 45232 (2017).
26. N. Nimer *et al.*, Bile acids profile, histopathological indices and genetic variants for non-alcoholic fatty liver disease progression. *Metabolism* **116**, 154457 (2021).
27. A. S. Devlin, M. A. Fischbach, A biosynthetic pathway for a prominent class of microbiota-derived bile acids. *Nat. Chem. Biol.* **11**, 685–690 (2015).
28. J. M. Ridlon, S. L. Daniel, H. R. Gaskins, The Hylemon-Bjorkhem pathway of bile acid 7-dehydroxylation: History, biochemistry, and microbiology. *J. Lipid Res.* **64**, 100392 (2023), 10.1016/j.jlr.2023.100392.
29. J. D. Sutherland, I. A. Macdonald, The metabolism of primary, 7-oxo, and 7 beta-hydroxy bile acids by Clostridium absonum. *J. Lipid Res.* **23**, 726–732 (1982).
30. H. L. Doden *et al.*, Completion of the gut microbial epi-bile acid pathway. *Gut Microbes* **13**, 1–20 (2021).
31. D. Shalon *et al.*, Profiling the human intestinal environment under physiological conditions. *Nature* **617**, 581–591 (2023).
32. R. A. Quinn *et al.*, Global chemical effects of the microbiome include new bile-acid conjugations. *Nature* **579**, 123–129 (2020).
33. J. M. Ridlon, D. J. Kang, P. B. Hylemon, Bile salt biotransformations by human intestinal bacteria. *J. Lipid Res.* **47**, 241–259 (2006).
34. D. R. Schmidt *et al.*, AKR1B7 is induced by the farnesoid X receptor and metabolizes bile acids. *J. Biol. Chem.* **286**, 2425–2432 (2011).